Selective cytotoxicity of the herbal substance Acteoside against tumor cells and its mechanistic insights

Christina Cheimonidi, Pinelopi Samara, Panagiotis Polychronopoulos, Eleni N. Tsakiri, Theodora Nikou, Vassilios Myrianthopoulos, Theodore Sakellaropoulos, Vassilis Zoumpourlis, Emmanuel Mikros, Issidora Papassideri, Aikaterini Argyropoulou, Maria Halabalaki, Leonidas G. Alexopoulos, Alexios-Leandros Skaltsounis, Ourania E. Tsitsilonis, Nektarios N. Aligiannis, Ioannis P. Trougakos

Supplementary Information

Supplementary Figures Legends

Figure S1. The multistage mouse skin carcinogenesis model as an experimental platform to screen for new anti-tumor agents. (A) Flow cytometry analysis of basal ROS levels in C5N and A5 cell lines; values refer to mean (n=3) fluorescence intensity. (B) Relative basal mRNA expression levels of proteostatic modules and antioxidant responses-related genes in C5N and A5 cells. (C) Relative (%) enzymatic activities of the CT-L/β5, C-L/β1 and T-L/β2 proteasome peptidase activities (C_1) and of lysosomal cathepsin B, L activities (C_2) in C5N and A5 cells. (D) Mean values of flow cytometry analyses (n=4) showing (%) early (Annexin V+) and late (PI-Annexin V+) apoptotic C5N and A5 cells. (E) Relative (%) cell survival of C5N and A5 cells following treatment with increasing concentrations of doxorubicin, H_2O_2, chloroquinone and PS-341 for 24 h. Bars, ± SD (n≥2). *, $P<0.05$; **, $P<0.01$.

Figure S2. Basal phosphorylation levels of cancer and immune response-related signaling pathways in the C5N and A5 mouse cell lines. Heat map (A) and relative phosphorylation levels (B; A5 *vs.* C5N cells) of the shown proteins. The list of phosphorylation sites studied is reported in Suppl. Table S1. Bars, ± SD (n≥2). *, P<0.05; **, P<0.01.

Figure S3. Phytochemical analyses and purification of acteoside. (A) ^{1}H-NMR (MeOD) spectrum of the residue obtained from the methanolic extract of *L. citriodora* after removal of non-polar compounds. (B) LC-HRMS chromatogram from *L. citriodora* methanolic extract. (C) Spectroscopic data [^{1}H-NMR (MeOD) (C_1) and HRMS (C_2) spectra] of purified acteoside.

Figure S4. Treatment of C5N and A5 cells with acteoside alters the phosphorylation pattern of major cancer and immune response-related signaling pathways. Heat map (A) and relative phosphorylation levels (B; treated *vs.* non treated cells) of the shown proteins. Bars, ± SD (n≥2). *, P<0.05; **, P<0.01.

Figure S5. Acteoside exerts increased toxicity in human cancer cell lines, shows synergistic effects with cytotoxic agents and re-sensitizes doxorubicin-resistant human cancer cells. (A) Relative (%) cell survival of human osteosarcoma cell lines after treatment with increasing concentrations of acteoside for 24 h. (B) Relative (%) cell death of the human osteosarcoma cell lines U2 OS, Sa OS and KH OS after treatment with 100 μM acteoside in the presence [or not (Con)] of the oxidant H_2O_2 (800 μM); the chemotherapeutic drug doxorubicin (DXR; 0.35 μM) or the proteasome inhibitor epoxomicin (Epox; 10 nM) for 24 h. (C) Relative fold of cell death enrichment of the human osteosarcoma cell lines U2 OS R1-R2, Sa OS R1 and KH OS R1-R3 that are resistant to increasing concentrations of doxorubicin [23] after treatment with 100 μM acteoside for 48 h. Bars, ± SD (n≥2). *, P<0.05; **, P<0.01.

Figure S6. Acteoside exerts cytotoxic effects and alters the phosphorylation levels of cancer and immune response-related pathways in B16 melanoma mouse cells. (A) Relative (%) cell survival of B16.F1 and B16.F10 mouse cancer cell lines after treatment (*vs*. control) with increasing concentrations of acteoside for 24 h. (B) Heat map (B_1) and relative basal (B_2; B16.F10 *vs.* B16.F1 cells) or after cell treatment (+) with 500 μM acteoside (B_3) phosphorylation levels of the shown proteins. Bars, ± SD (n≥2). *, P<0.05; **, P<0.01.

Figure S7. Acteoside exerts no cytotoxic effects in normal human diploid fibroblasts. (A_1) Representative phase contrast images of pre-senescent human fibroblasts (IMR90 cells) after exposure, or not (Con), to 100 μM acteoside for 3 weeks. (A_2) Relative (%) cell number after completion of treatment. (B_1) Representative light field images following *SA-β-gal* staining of cells cultured in the presence, or not (Con), of 100 μM acteoside for 3 weeks. (B_2) Relative (%) number of *SA-β-gal* positive cells (mean of 10 optical fields) following treatment of cells exactly as in (B_1). Bars, ± SD (n=2). *, P<0.05.

Figure S8. Acteoside was not cytotoxic after dermal application in Wistar rats and alleviated the toxic effects of doxorubicin. (A_1) Sites of doxorubicin injection in Wistar rats. (A_2) Representative photographs of animals treated with acteoside (Acteo), doxorubicin (DXR) and doxorubicin/acteoside (DXR/Acteo) for 6 weeks. (B) Mean weight (Kg) of rats treated with acteoside, doxorubicin and doxorubicin/acteoside as in (A); the number of deaths per treatment group are also indicated. Bars, ± SD (n≥2). *, P<0.05.

Figure S9. Lifetime oral administration of acteoside in *Drosophila melanogaster* flies was not toxic and offered mild protection against proteotoxic stress. (A) Longevity curves of flies exposed [or not (Con)] to 800 μM acteoside. (B, C) Longevity curves of flies exposed to the oxidant t-BHP (B) or to the proteasome inhibitor PS-341 (C) in the presence or absence of the shown concentrations of the compound. Statistical analyses of the indicated experiments are reported in Suppl. Table S2.

Figure S10. *In vivo* administration of acteoside alters the phosphorylation pattern of major cancer and immune response-related signaling pathways in the tumor. (A) Representative immunoblot analyses in dissected tumors from control and acteoside-treated (IP or OR) mice, probed with antibodies against β5, Beclin, Nrf-2, Ku70, PKC and proteome carbonylation (DNP); GAPDH probing was used as reference. (B) Heat map (B_1) and relative phosphorylation levels (B_2) in dissected tumors after acteoside administration either intraperitoneally (IP) or *via* drinking water (OR). Con-1, Con-3, IP-1, IP-3 and OR-1, OR-3 represent samples from different animals; in (B_2) the means of all treated animals/assay are shown. Bars, ± SD ($n \geq 2$). *, $P<0.05$.

Figure S11. siRNA-mediated *pkc-α* gene expression knock down decreased cell survival in C5N, A5 and B16.F1 cells. (A_1) Q-RT-PCR assay of *pkc-a* gene expression levels in C5N, A5 and B16.F1 cells after treatment with acteoside (500 μM) for 48h, or after transfecting (or not) cells with *pkc-a* RNAi oligonucleotides. (A_2) Representative immunoblot analyses of protein samples probed with PKC antibody after *pkc-a* RNAi for 48 h in C5N, A5 and B16.F1 cells. GAPDH probing was used as reference. (B) Relative (%) cell survival of C5N, A5 and B16.F1 cells after treatment with acteoside (500 μM) for 48h or following transfection (or not) with *pkc-a* RNAi oligonucleotides. Bars, ± SD ($n \geq 2$). *, $P<0.05$; **, $P<0.01$.

Figure S12. Multiple alignment of PKC α, β and γ isoforms (UniProt accession codes: P17252, P05771, P05129, respectively). The shown alignment denotes the high degree of similarity between the three isoforms (62.54% identity, 81.62% similarity). Amino acids that are identical are shown in red boxes; similar amino acids are indicated by red letters. The enzyme gatekeeper position is indicated by a green arrow.

Supplementary Materials and Methods

Purification of acteoside

The insoluble material after extraction of the dried *Lippia citriodora* leaves (10 g) was subjected to countercurrent chromatography using a fast centrifugal partition chromatograph (FCPC) apparatus (Kromaton, France) equipped with a rotor of 1000 mL designed with 45 discs, each one having 32 Z-shaped cells yielding a total of 1440 cells. A mixture of EtOAc/EtOH/H_2O at ratio 5/0.5/4.5 was used

as biphasic solvent system. The solvents were thoroughly mixed in a separating funnel at room temperature prior to use and the two phases were separated after equilibration of the mixture. After filling with the stationary phase (lower phase), rotation was set at 800 rpm and the mobile phase was pumped through the system at a flow rate of 15 mL/min. The solvent was pumped through the system with a preparative pump LabAlliance and the sample was injected *via* a 30 mL sample loop. Initially, the organic phase was used as mobile phase in "ascending'' mode and 120 fractions (50 mL per fraction) were collected. Subsequently, the mode was changed to "descending" and the aqueous phase was used as mobile phase, resulting in 30 more fractions (50 mL per fraction). All fractions were subjected to Thin Layer Chromatography; then the chromatograms were observed under a UV lamp (254 and 365 nm) and visualized by spraying with methanol vanillin sulfate followed by heating for two minutes. A total of 2.1 g of acteoside (purity ≥ 90%) was isolated by the aforementioned process. The identification of acteoside was performed by nuclear magnetic resonance (NMR) and mass spectrometry (MS) spectra, while its purity was established by UPLC-MS and NMR analysis.

UPLC-HRMS analysis (evaluation of the isolated acteoside purity)

An ACQUITY UPLC BEH C18 (2.1×100 mm, 1.7 μm) reversed phase column (Waters Corp., Milford, MSA, USA) preceded by a precolumn (Waters VanGuard 5 x 2.1 mm, 1.7 μm) was used for the chromatographic separation. The mobile phase consisted of solvents A: aqueous-0.1% (v/v) formic acid and B: methanol-0.1% (v/v) formic acid. The initial conditions were 100% A for 2 min, adjusting to 100% B in 15 min. This solvent composition was maintained for 5 min (100% B) followed by return to initial conditions and a re-equilibration step (2 min) prior to next run. Flow rate and column temperature were kept at 0.40 mL/min and 50°C, respectively, while the autosampler tray temperature was set at 4°C and injection volume to 10 μL. A hybrid HRMS (LTQ-Orbitrap Discovery) operated separately in ESI-negative ion mode was used. Capillary temperature, capillary voltage and spray voltage were set at 356°C, 20 V and 3.10 kV, respectively. Analysis was performed using the Fourier transform (FT) MS full scan ion mode, applying a resolution of 30 000, while acquisition of the mass spectra was performed in every case using the centroid mode.

NMR analysis (identification of isolated acteoside)

NMR spectra of crude plant extract and purified acteoside were recorded at 400 and 600 MHz (Advance III 600 MHz; Bruker, Karlsruhe, Germany) in MeOD. Chemical shifts are reported in ppm δ and referred to the residual solvent signal; J (coupling constant) are given in Hz. 2D-NMR experiments, including COSY, HSQC and HMBC were performed for the elucidation of the structure of acteoside using standard Brucker microprograms.

Sample preparation for UHPLC-MS analyses of biological samples (plasma and dissected tumors)

In total, 12 plasma samples (3 from control mice, 5 after acteoside administration *via* the IP route and 4 after acteoside administration *via* the OR route) and 9 samples from dissected melanoma tumors (3 from control mice, 3 after acteoside administration *via* the IP route and 3 from mice where acteoside was delivered orally) were analyzed; samples were kept frozen at -80^{o}C before analysis. The preparation was performed as described previously (Wen et al., 2016).

Briefly, after thawing plasma samples at 4^{o}C they were vortexed to achieve homogenization and 50 µL of plasma were mixed with 400 µL of cold acetonitrile. The acquired solutions were then centrifuged at 12 000×g (10 min, 4^{o}C); the supernatant was diluted with 550 µL of water and 50 µL of internal standard (IS) and was then directly injected for UHPLC-MS analysis. The whole procedure was carried out on ice.

For extraction of dissected tumors ~50 mg of thawed tissue were weighted. Tumors were then dissolved in 1 mL cold acetonitrile, homogenized and vortexed for 1 min. Samples were transferred to a sonication bath for 20 min at 25^{o}C and centrifuged at 12 000×g for 10 min at 4^{o}C. The obtained supernatants were evaporated under vacuum conditions and then dissolved in 90 µL acetonitrile, 50 µL water and 10 µL IS for UHPLC-MS analysis.

UHPLC-MS analyses for the identification of acteoside in mouse plasma and dissected grafted tumors

Quantification of acteoside was performed using on an Advance™ UHPLC system coupled to an EVOQ™ Elite Triple Quadrupole Mass Spectrometer (Bruker) equipped with a heated electrospray ionization source (HESI). The mobile phase was consisted of a gradient system with water and 0.1% (v/v) formic acid (A) and acetonitrile (B); the flow rate was set at 0.4 mL/min. Total analysis time was 12 minutes and the used chromatographic separation column was an Acquity® UPLC HSS T3 (Waters) (18 µm, 2.1 x 200 mm) heated at 40^{o}C. The elution system started with 2% B, reached 30% B in 5 min and remained in these conditions for 1 min. After 0.5 minutes B increased to 100 % where it remained for 1.5 minutes, before returning to the initial conditions for 4 min for equilibrium of the column. The injection volume was 5 µL and during analysis samples were kept at 10^{o}C.

Samples were ionized in negative mode with an ion spray voltage at 4000 V. The mass spectrometric parameters were: cone temperature, 250^{o}C; cone gas flow, 25 units; heated probe temperature, 300^{o}C; probe gas flow, 50 units; nebulizer gas flow, 50 units. The quantification of acteoside was conducted employing multiple reaction monitoring (MRM) mode and suitable collision energies. The optimized parameters were established after direct infusions of acteoside and IS standard solutions of 1 µg/mL. For acteoside the following transitions were monitored: 623.4>161.1, collision energy:31 as confirmation transition and 623.4>133.2, collision energy:38; 623.4>461.3, collision energy:27 as quantification transitions. The above transitions were monitored from 3-5 min. For luteolin the following transitions were monitored: 285.3>133.1, collision energy:29; 285.3>151.0 collision energy:23 as confirmation and quantification transitions, respectively monitored for 5-7 min. Data were collected in centroid mode.

UHPLC-MS analyses for the quantification of acteoside in mouse plasma and grafted tumors

For acteoside quantification a standard calibration curve was built using eight different acteoside concentrations (i.e. 5, 10, 15, 20, 30, 40, 70 and 100 ng/mL) as described before (Wu et al., 2006) with minor modifications. The construction of the calibration curve (luteolin was used as IS) was based on the ratio area of acteoside/IS *vs.* the known concentrations of acteoside. Linearity was evaluated by coefficient of determination (R^2) from the linear regression using the least squares approach. All concentration levels were measured in triplicates. Blank samples were re-injected every three injections in order to avoid carryover effect of the different concentration levels.

Cell lines and cell culture conditions

Human lung embryonic fibroblasts (IMR90 cells) were maintained in Dulbecco's modified Eagle's medium (DMEM; Gibco Life Technologies), supplemented with 10% (v/v) fetal bovine serum (FBS), 2 mM glutamine and 1% non-essential amino acids in a humidified incubator at 5% CO_2, 37°C. Cells were subcultured at a split ratio 1:2 (when confluent) using trypsin/EDTA solution (Gibco Life Technologies). All other cell lines were cultivated in DMEM (Gibco Life Technologies), supplemented with 10% (v/v) FBS and 2 mM L-glutamine in a humidified incubator at 5% CO_2, 37°C and were subcultured with the use of trypsin/EDTA solution.

Cytotoxicity assay and assessment of cell death

Cells were seeded in 96-well plates and let to adhere overnight; the next day, cells were treated for 24 h with different concentrations of the agent in test. The MTT cytotoxicity assay was performed as described previously [26].

To assess apoptosis by FACS, cells were treated with acteoside for 24 h and the Annexin V Apoptosis Detection kit with Propidium Iodide (PI) (Biolegend) was used to identify apoptotic and necrotic cells; assays were performed according to the manufacturer's instructions. Briefly, cells were detached, washed twice with PBS and resuspended in Annexin V binding buffer (10^6 cells/mL). 100 µL of cell suspension were transferred in FACS tubes, where 5 µL of FITC Annexin V and 10 µL of PI were added; cells were then vortexed and incubated for 15 min in the dark. 400 µL of Annexin V binding buffer were added to each tube and cells were immediately analyzed in a FACSCanto II flow cytometer using FACSDiva software (BD Biosciences).

RNA extraction from cells or dissected tissues, cDNA synthesis and Real-Time PCR

The TRI Reagent (Sigma-Aldrich) was used for total RNA isolation from cells. RNAlater (Sigma-Aldrich) and the RNeasy mini kit (Qiagen) were used for total RNA isolation (as per manufacturer's instructions) from tumors dissected from acteoside treated mice. Isolated (1 µg) RNA was converted to cDNA by the usage of Maxima First Strand cDNA Synthesis Kit for RT-qPCR (Thermo Scientific). Quantitative Real-time PCR was performed in a Piko Real 96 Real-Time PCR System (Thermo

Scientific). Primers were designed using the primer-BLAST tool (http://www.ncbi.nlm.nih.gov/tools/primer-blast/) and were the following:
a7-F: ATCAACAGAGCCCGGGTAGA, *a7*-R: GCCGAGATACCAAATGGCCT;
β5-F: AATGCTTCACGGAACCACCA, *β5*-R: CTTCACCGTCTGGGAAGCAA;
rpn6-F: TCCATTGATAGCCCCAAGGC, *rpn6*-R: CTGCATACCGAAGTGCAAGC;
rpn11-F: ACACCTGAACAGCTGGCAAT, *rpn11*-R: ATCCAACATTGCGGCCAAAC;
β2-F: AACCTGGCTGACTGTCTTCG, *β2*-R: GGCCCTTCATGCTCGTCATA;
β1-F: AGTTAGGCGCGATGCTTTCC, *β1*-R: ACAGTACCTCCGTTGAAGGC;
ctsl-F: AATGGAGGTCTGGACTCGGA, *ctsl*-R: CAGCGAACTCGGCTCTGTAT;
beclin1-F: GGAAGTAGCTGAAGACCGGG, *beclin1*-R: TTAGACCCCTCCATGCCTCA;
lc3β-F: GCTCGCTGCTGTCTAGATGT, *lc3β*-R: CAGTCGCTTAAGCTGGGTCA;
hdac6-F: TCAGCCTCAACTGGTCTTGG, *hdac6*-R: AGCAAATGGGTTAGGTGGGC;
clusterin-F: GCAGGAGGTCTCTGACAATGA, *clusterin*-R: GACGGCGTTCTGAATCTCCT;
nrf2-F: CCAGGACTACAGTCCCAGCAG, *nrf2*-R: CTCCAAGATCTATGTCTTGCCTCC;
keap1-F: CATTGGCATCGCCAACTTCG, *keap1*-R: CCTCCCCGAAGTGCATGTAG;
txnrd1-F: CCATCGGTGACATCCTGGAG, *txnrd1*-R: CTCTGAGCCAGCAATCTCCC;
nqo1-F: CAT-TGC-AGT-GGT-TTG-GGG-TG, *nqo1*-R: TCTGGAAAGGACCGTTGTCG;
gsk3a-F: CAGAGACGAGGGAACTGGTG, *gsk3a*-R: CAGTGGTCCAGCTTACGCA;
gsk3β-F: TAGTCGAGCCAAGCAGACAC, *gsk3β*-R: TGTCTCGATGGCAGATTCCAA;
stub1-F: TGAAGATGCAGCAGCCTGAA, *stub1*-R: AAGAAGTGCGCCTTCACAGA;
pdk1-F: ACGGGACAGATGCGGTTATC, *pdk1*-R: GCTTCCAGGCGGCTTTATTG;
pdp2-F: AGGAGAGGACGAGGATACGAG, *pdp2*-R: CTCCCACCTCGTAAAAGAGCA;
pkm-F:TGATAGTTCTCACGGAGTCTGG, *pkm*-R: ACAGGGAAGATGCCACGGTA;
pklr-F: GGCAGATGATGTGGACCGAA, *pklr*-R: CCAGATCACCAACTCGGAGG;
foxo3-F: GGTACCAGGCTGAAGGATCA, *foxo3*-R: CGTGGGAGTCTCAAAGGTGT;
foxo1-F: TCAAGGATAAGGGCGACAGC, *foxo1*-R: CCTCCCTCTGGATTGAGCATC;
chop-F: GCATCTTCATACACCACCACAC, *chop*-R: GGTGAAAGGCAGGGACTCAG;
grp78-F: GGAAAGAAGGTTACCCATGC, *grp78*-R: AGAAGAGACACATCGAAGGT;
pepck-F:AAGAAGAAATACCTGGCCGCA, *pepck*-R: TTTGTCTTCACTGAGGTGCCA. β-actin was used as a normalizer. *β-actin*-F: GGCTGTATTCCCCTCCATCG, *β-actin*-R: CCAGTTGTTAACAATGCCATGT.

siRNA transfection experiments

Cells were transfected for 48 h using DharmaFECT Transfection reagent, as well as the SMARTpool ON-TARGET plus PKCa siRNA (L-040348-00-0005) or the ON-TARGET plus non-targeting pool (siCtrl) (D-001810-10-05) (GE Healthcare Dharmacon Inc.) according to manufacturer's instructions.

Immunoblot analysis and detection of protein carbonyl groups

For immunoblotting analyses, primary and secondary antibodies were applied for 1 h at room temperature, and immunoblots were developed using an enhanced chemiluminescence reagent kit (GE Healthcare Amersham, Buckinghamshire, UK). Primary antibodies against β5 (sc-55009), Beclin (sc-59570), Nrf-2 (sc-722), Ku70 (sc-1487), PKC (sc-80) and GAPDH (sc-25778), along with the secondary HRP-conjugated antibodies, were purchased from Santa Cruz Biotechnology.

For the detection of protein carbonyl groups, the OxyBlot protein oxidation detection kit (Millipore, Billerica, MA; S7150) was used. Carbonyl groups in protein side chains of each sample reacted with 2,4-dinitrophenylhydrazine (DNPH) and produced 2,4-dinitrophenylhydrazone (DNP-hydrazone); DNP was then detected by a specific antibody.

Measurement of proteasome and cathepsin B, L peptidase activities in cell or tissue lysates

Measurement of proteasome or lysosomal cathepsin B, L peptidase activities in cell lysates was performed as described before [26]. For measuring proteasome or cathepsin B, L peptidase activities in isolated tumor biopsies, dissected tumors were lysed in a specific phosphoprotein buffer (ProtAtOnce) containing protease and phosphatase inhibitors (Sigma-Aldrich). Total protein content was assayed with Bradford (Bio-Rad Laboratories) and peptidase activities were measured as described [26]. Hydrolysis of the fluorogenic peptides was recorded (excitation, 350 nm; emission, 440 nm) in a Versa Fluor^{TM} Fluorometer System.

Measurement of Reactive Oxygen Species

Cells were treated with acteoside for 24 h, trypsinized and incubated for 30 min at 37^{o}C with the CM-H_2DCFDA dye (Invitrogen). The resulting fluorescence was monitored by flow cytometry using a FACSCanto II cell analyzer as described previously (Samudio et al., 2005).

Gelatin zymography for assessing matrix metalloproteinase (MMP)-2 and MMP-9 activity

Acrylamide gels (SDS–PAGE, 12%) were supplemented with gelatin (1 mg/mL). Cell culture supernatant was collected 24 h post-treatment with acteoside and 25 μL were loaded on SDS gels along with 2X non-reducing Laemmli buffer. After electrophoresis, gels were washed in a buffer containing 2.5% Triton X-100, 50 mM Tris–HCl (pH 7.4) and 5 mM $CaCl_2$ for 1 h and were placed on an orbital shaker. Gels were then incubated for 24 h at 37°C in a buffer containing 5 mM $CaCl_2$, 50 mM Tris–HCl pH 7.4 and stained in a Coomassie Brilliant blue solution (0.25% Coomassie blue, 30% methanol, 10% acetic acid) for 3 h, followed by gel destaining with 30% methanol and 10% acetic acid. The position and related enzymatic activities of MMP-2 and MMP-9 were observed as clear bands over the blue background.

Phosphoproteomic analysis

Cells or dissected tumors extracts were lysed with the use of a specific phosphoprotein buffer (ProtAtOnce) containing protease and phosphatase inhibitors (Sigma-Aldrich). The Bradford method (Bio-Rad Laboratories) was used to assess protein content of samples. Equal amount of proteins was then used to analyze the phosphoproteomic profile of the samples under study by Luminex technology (xMAP technology-ProtAtOnce). The phosphoproteomics panel has been described previously (Melas et al., 2014) and is also reported in Suppl. Table S1.

PKC kinase assay

PKC kinase activity was measured using a PKC Activity Assay Kit (AbCam). Briefly, cells were plated in 60 mm dishes (500 x 10^3 cells/mL) and were let to adhere overnight; 24 h post-compound treatment, cells were lysed and PKC activity was measured as per manufacturer's instructions. The effect of acteoside against purified PKC (obtained from the PKC kit) activity after immunoprecipitation of cellular PKC or in cell lysates was also assayed.

Senescence-associated β-galactosidase staining

Pre-senescent human fibroblasts were treated for 3 weeks with 100 μM of acteoside followed by *β*-galactosidase staining, as previously described (Debacq-Chainiaux et al., 2009). Briefly, cells were washed with PBS and fixed in 0.2% glutaraldehyde and 2% formaldehyde in PBS for 5 min. After fixation, cells were washed with PBS and stained (in the absence of CO_2) for 12-16 h at 37°C in staining solution [150 mM NaCl, 2 mM $MgCl_2$, 5 mM $K_3Fe(CN)_6$, 5 mM $K_4[Fe(CN)_6].3H_2O$, 40 mM citric acid/sodium phosphate, pH 6.0, containing 1 mg/mL 5-bromo-4-chloro-3-indolyl-*β*-d-galactoside]. Cells were viewed under phase contrast optics in a TS-100F NIKON inverted microscope and at least 10 optical fields were used to score positively stained cells.

Fly culture and longevity assay

Flies stocks were maintained at 23°C, 60% relative humidity on a 12 h light:12 h dark cycle and were fed standard medium. The *D. melanogaster* flies used in this study were the wild type strain Oregon-R. For longevity assays, 1-3 days old female and male flies were transferred to vials (for the number of flies used per assay, see Suppl. Table S2). Flies were transferred to fresh culture medium or to compound/drug-containing culture medium (experimental conditions for each group are indicated in figure legends) every 3 days. The number of dead flies was recorded daily. Survival curves were analyzed by Kaplan-Meier and log-rank test; statistical analysis of each lifespan experiment is presented in Suppl. Table S2.

Treatment of Wistar rats

Wistar rats (n=20, ~0.32 Kg of weight, 2 weeks of age) were obtained from the Hellenic Pasteur Institute and housed under controlled temperature (22°C) and photoperiod (12 h light:12 h dark) with free access to water and food. Animals were separated in three groups. In the first group, animals

(n=4) were treated with only acteoside (*via* oral gavage) five times a week (126 mg/Kg). In the second group, animals (n=8) were treated with doxorubicin *via* subcutaneous (sc) injection once a week (4 mg/Kg) at different areas to avoid tissue necrosis. The animals of the third group (n=8) were treated with both doxorubicin and acteoside. Animal behavior, weight and any notable signs of toxicity (or deaths) were monitored daily for a total period of 6 weeks.

Docking calculations and molecular simulations via a stepwise docking protocol

The crystal structure of human PKC α isoform in complex with a ligand (pdb id: 4RA4) was utilized for docking calculations. The multiple alignment of the α, β and γ isoforms of the kinase (UniProt accession codes: P17252, P05771, P05129, respectively) was performed using the on-line module Clustal-O available at UniProt and showed that the three proteins share a high degree of sequence similarity (62.54% identity, 81.62% similarity; see Suppl. Fig. S12). As a first step, rigid docking of acteoside to the kinase ATP binding pocket was performed using the Glide SP algorithm. A number of poses were obtained and were ranked on the basis of their binding affinity as predicted by the GScore scoring function. Further, the top-ranked poses were rescored utilizing a flexible representation of the studied system and the interaction energy was determined for each pose using MacroModel and the Embrace docking module. The aforementioned protocol enabled for enhanced sampling of ligand conformations at the docking stage, due to the efficacy of the Glide search algorithm, while at the same time, it allowed for optimal scoring of protein-ligand interactions by considering the studied system flexibility and a linear interaction energy approach involving intermolecular electrostatic and Van der Waals energy terms as implemented in Embrace (Friesner et al., 2004; Friesner et al., 2006; Halgren et al., 2004). The resulting geometries and corresponding energies were then used to perform a Boltzmann population analysis and six distinct poses accounting for 95.4% of the total population were determined. Top-ranked poses, ranging within 2 kcal/mol from the global minimum were subjected further to rescoring by utilizing the flexible docking MacroModel Embrace minimization algorithm. The interaction energy mode with OPLS2005 force-field, a distance-dependent dielectric constant of 4 and the TNCG minimization algorithm were used. The Boltzmann populations of the derived poses were calculated at 300°K.

Statistical Analysis

All experiments were performed at least in duplicates (unless otherwise stated in Figure legends) and data were statistically analyzed with the use of ANOVA single factor. For statistical analysis of flies' lifespan, the Statistical Package for Social Sciences (IBM SPSS; version 19.0 for Windows, NY, USA) was used. Data points correspond to the mean of the independent experiments and error bars denote standard deviation (SD).

Supplementary References

F. Debacq-Chainiaux, J.D. Erusalimsky, J. Campisi, O. Toussaint, Protocols to detect senescence-associated beta-galactosidase (SA-betagal) activity, a biomarker of senescent cells in culture and *in vivo*, Nat. Protoc. 4 (2009) 1798–1806.

R.A. Friesner, J.L. Banks, R.B. Murphy, T.A. Halgren, J.J. Klicic, D.T. Mainz, et al., Glide: A new approach for rapid, accurate docking and scoring. 1. Method and assessment of docking accuracy. J. Med. Chem. 47 (2004) 1739-1749.

R.A. Friesner, R.B. Murphy, M.P. Repasky, L.L. Frye, J.R. Greenwood, T.A. Halgren, et al., Extra precision Glide: Docking and scoring incorporating a model of hydrophobic enclosure for protein-ligand complexes. J. Med. Chem. 49 (2006) 6177–6196.

T.A. Halgren, R.B. Murphy, R.A. Friesner, H.S. Beard, L.L. Frye, W.T. Pollard et al., A new approach for rapid, accurate docking and scoring. 2. Enrichment factors in database screening. J. Med. Chem. 47 (2004) 1750–1759.

I.N. Melas, A.D. Chairakaki, E.I. Chatzopoulou, D.E. Messinis, T. Katopodi, V. Pliaka, et al., Modeling of signaling pathways in chondrocytes based on phosphoproteomic and cytokine release data. Osteoar. Cartil. 22 (2014) 509–518.

I. Samudio, M. Konopleva, N. Jr. Hail, Y.X. Shi, T. McQueen, T. Hsu, et al., 2-Cyano-3,12-dioxooleana-1,9-dien-28-imidazolide (CDDO-Im) directly targets mitochondrial glutathione to induce apoptosis in pancreatic cancer. J. Biol. Chem. 280 (2005) 36273–36282.

Y. Wen, S. Huo, W. Zhang, H. Xing, L. Qi, D. Zhao, N. Li, J. Xu, M. Yan, X. Chen, Pharmacokinetics, Biodistribution, Excretion and Plasma Protein Binding Studies of Acteoside in Rats. Drug Res. 66 (2016) 148-153.

Y.T. Wu, L.C. Lin, J.S. Sung, T.H. Tsai, Determination of acteoside in *Cistanche deserticola* and *Boschniakia rossica* and its pharmacokinetics in freely-moving rats using LC-MS/MS. J. Chromatogr. B Analyt. Technol. Biomed. Life Sci. 844 (2006) 89–95.

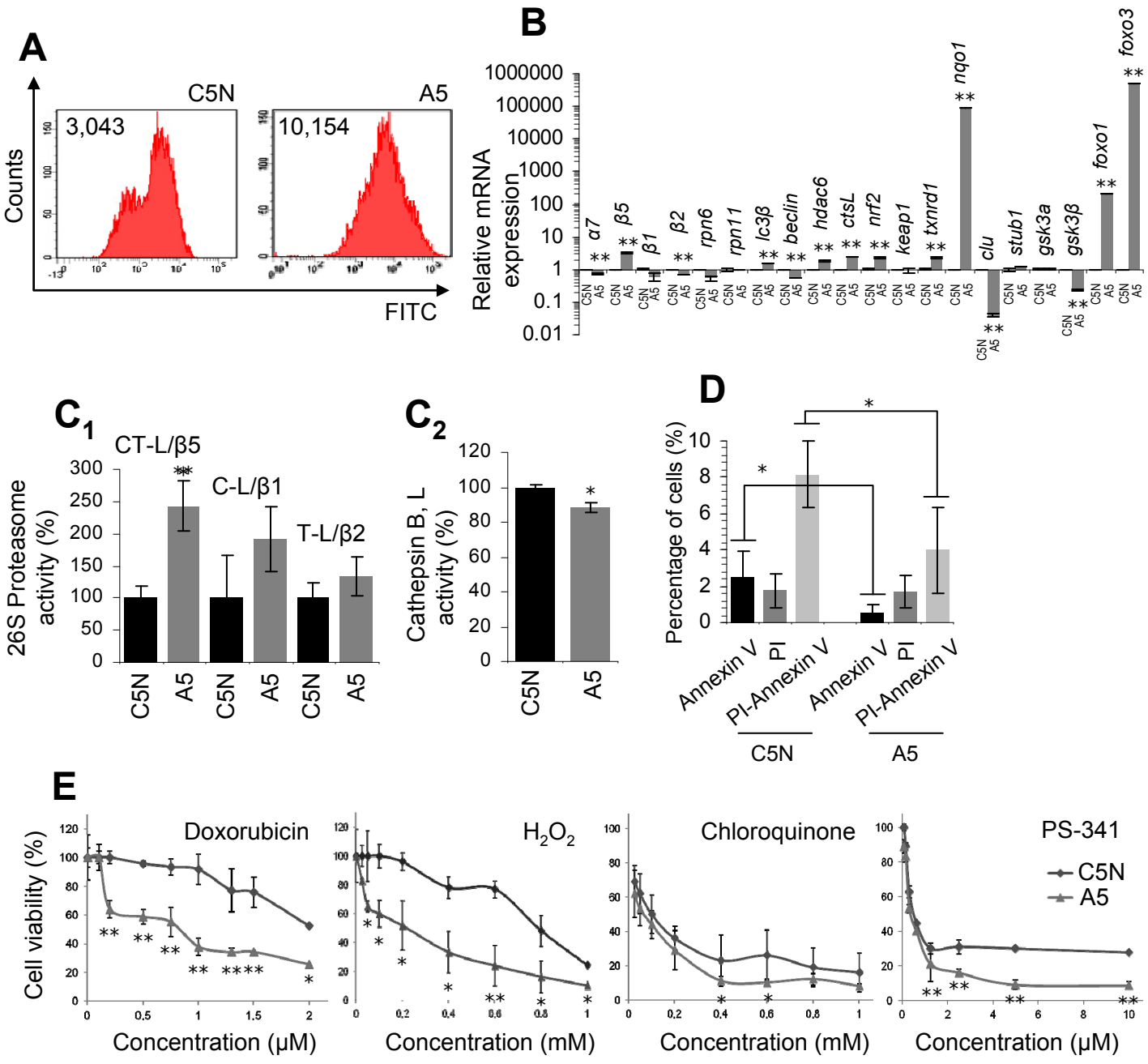

Cheimonidi et al. Fig. S1

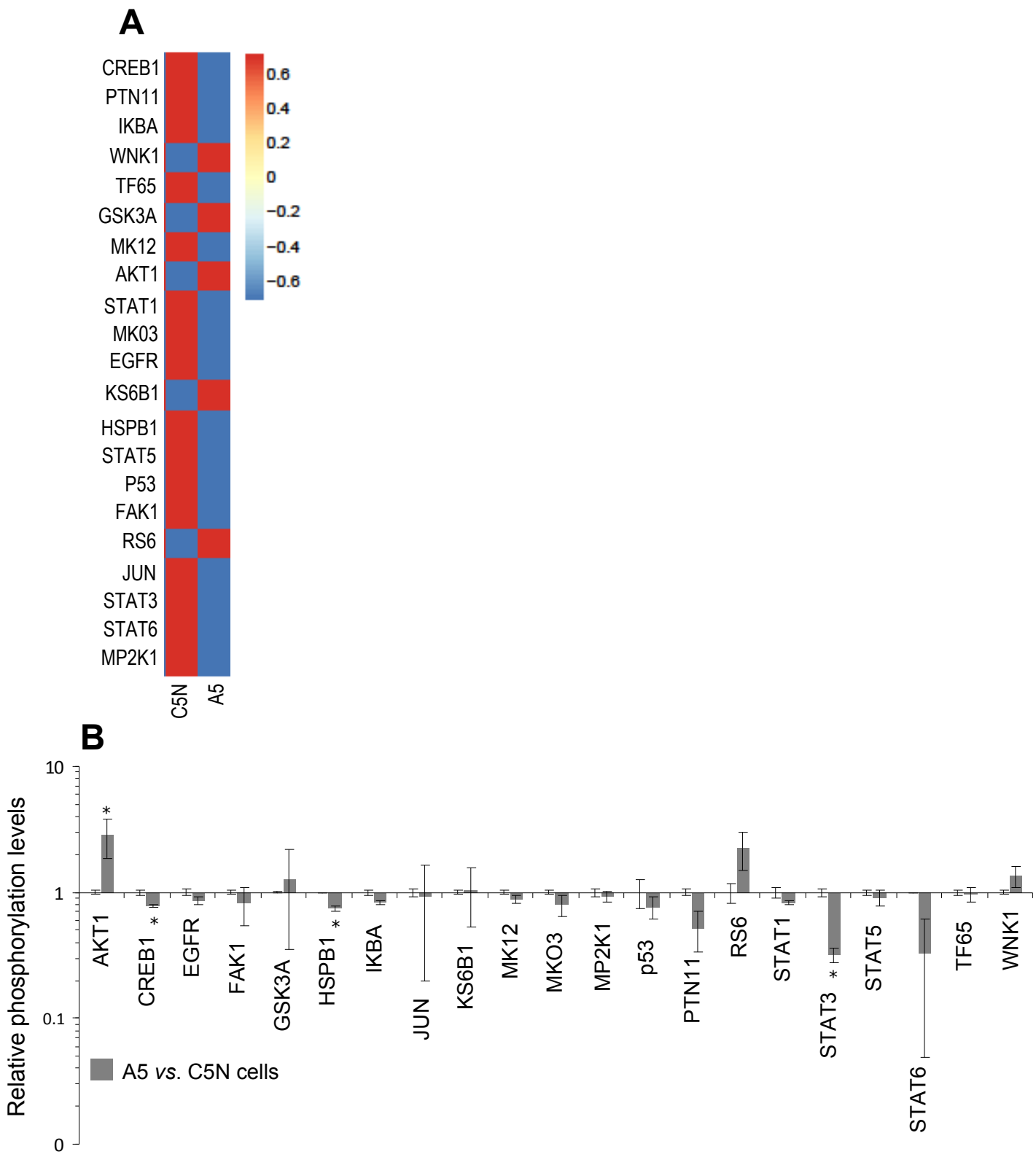

Cheimonidi et al. Fig. S2

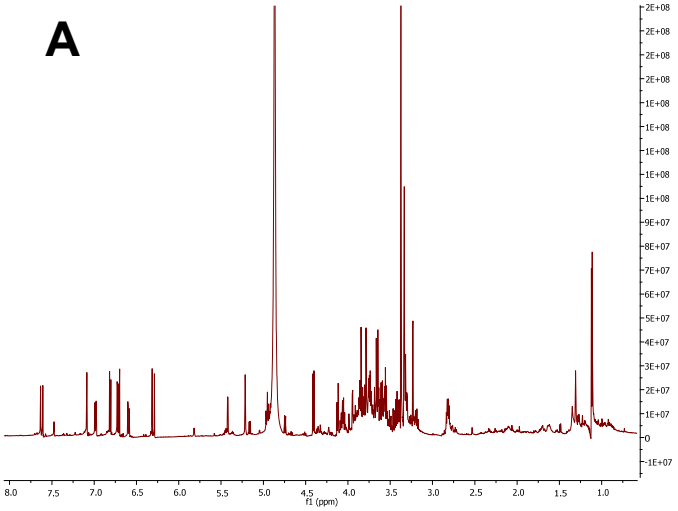

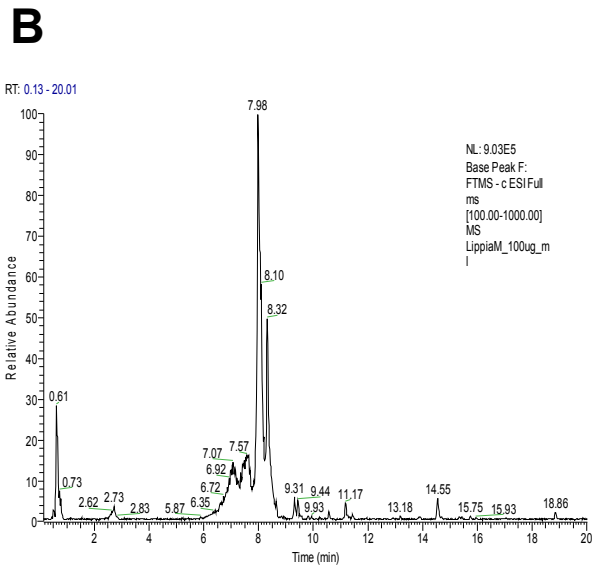

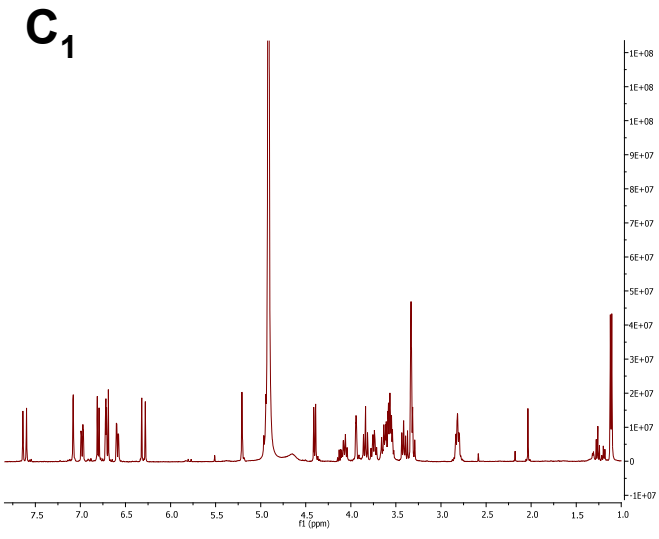

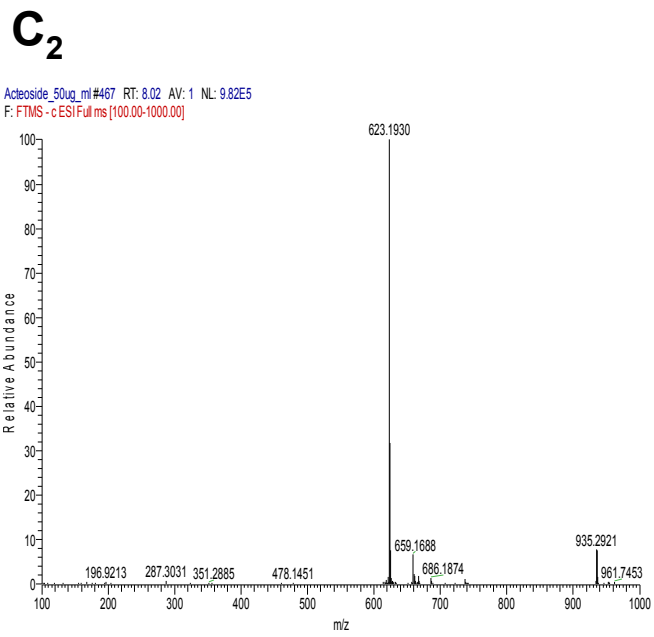

Cheimonidi et al. Fig. S3

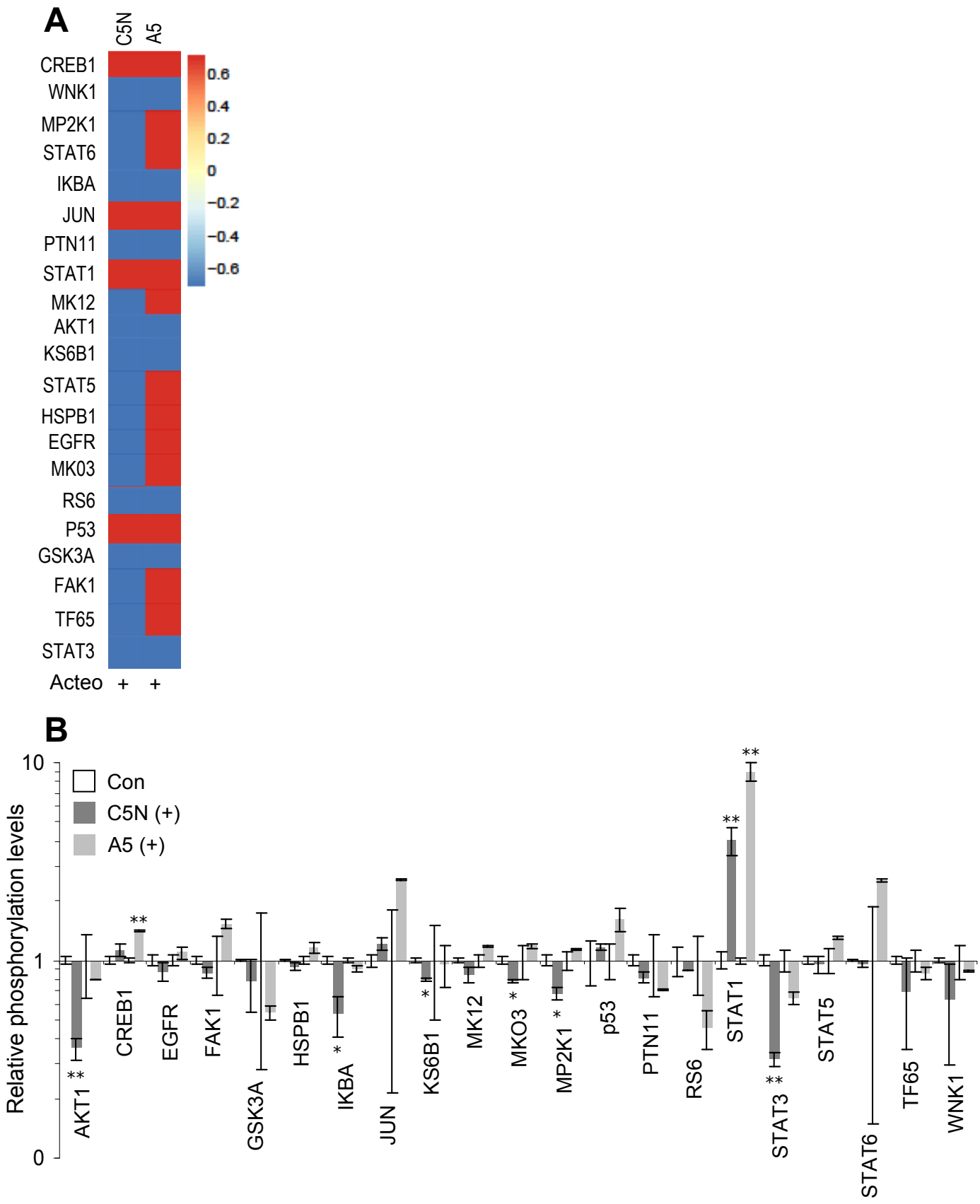

Cheimonidi et al. Fig. S4

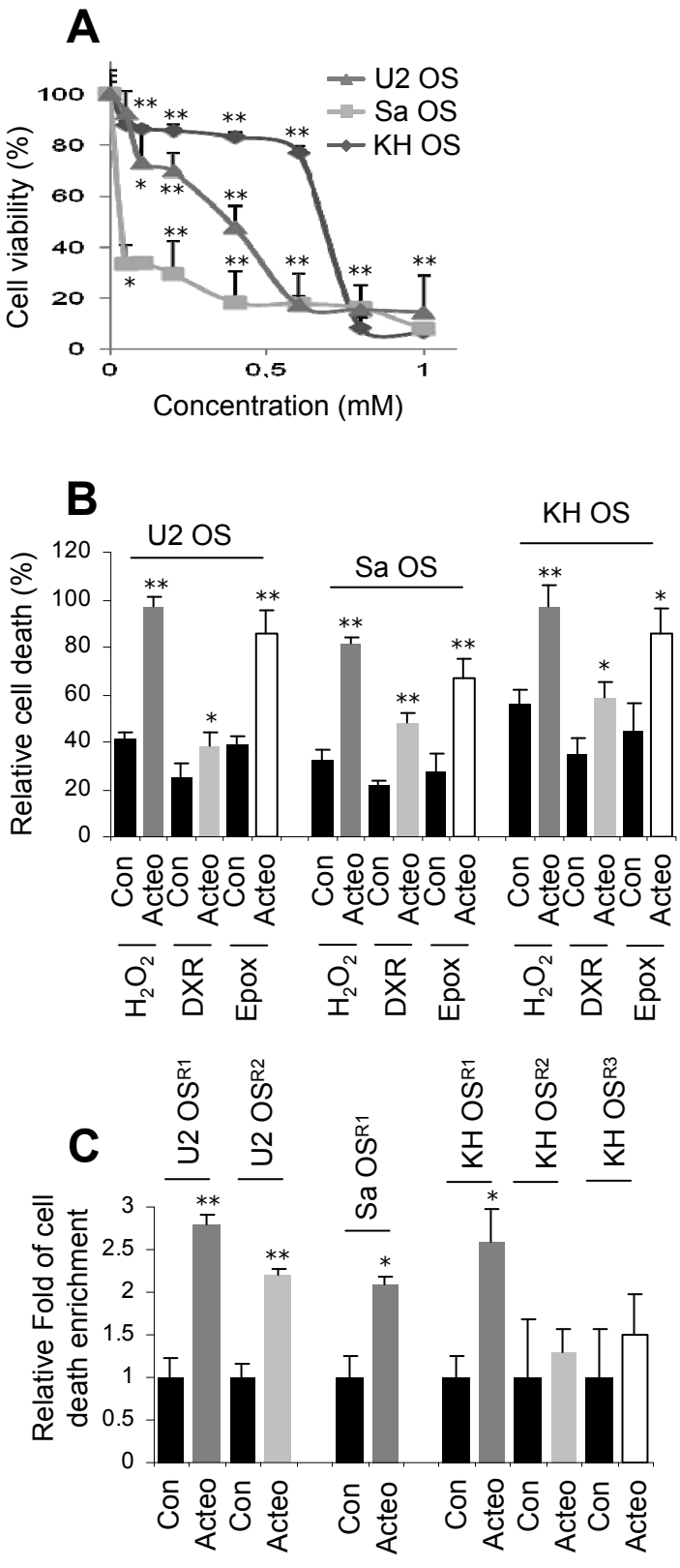

Cheimonidi et al. Fig. S5

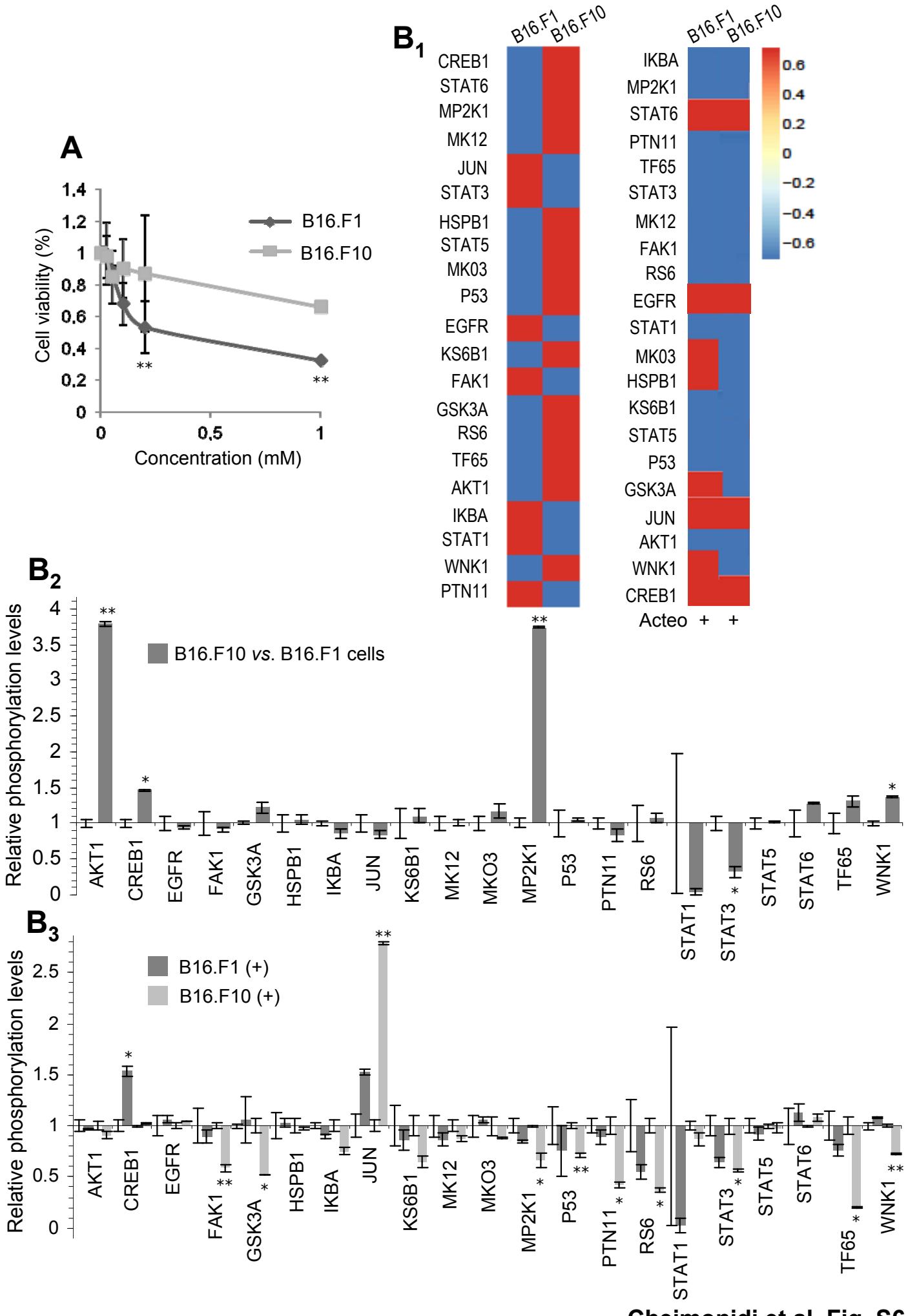

Cheimonidi et al. Fig. S6

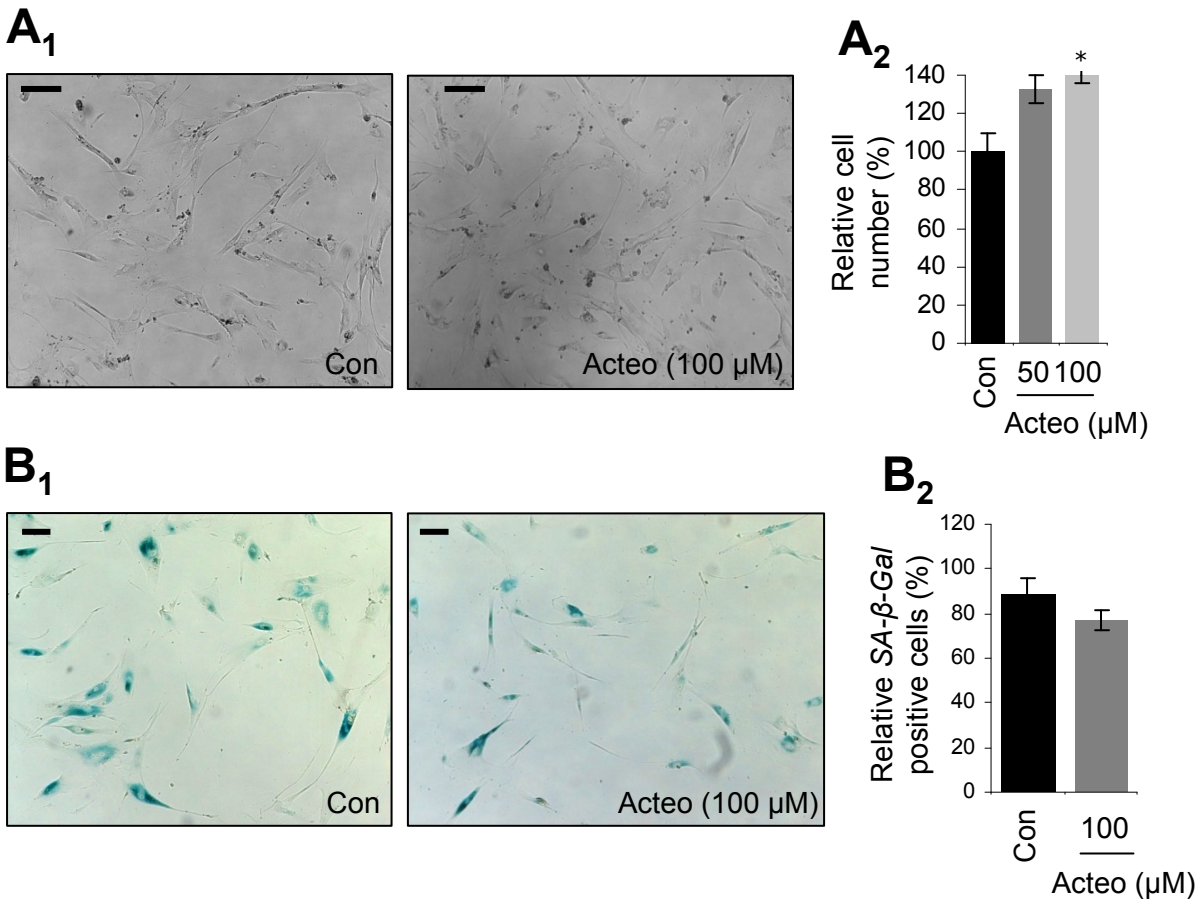

Cheimonidi et al. Fig. S7

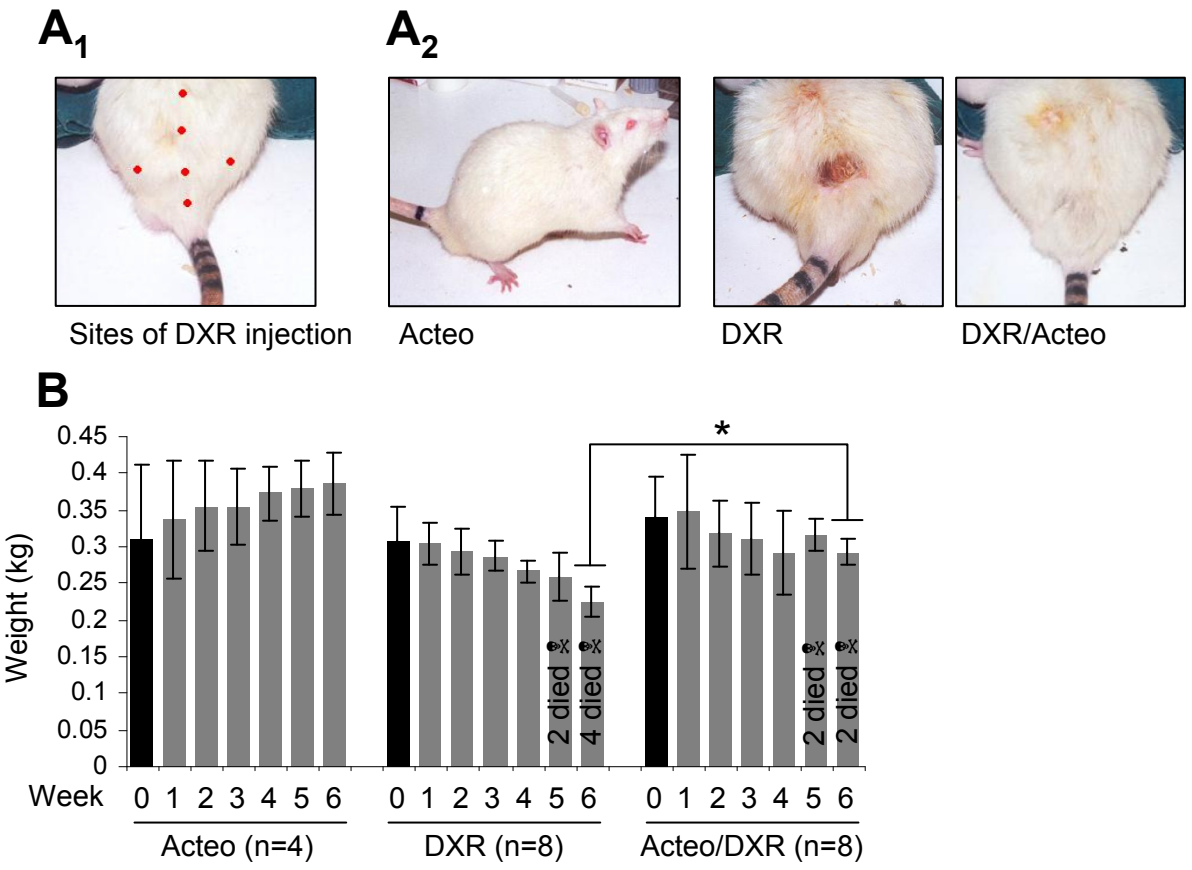

Cheimonidi et al. Fig. S8

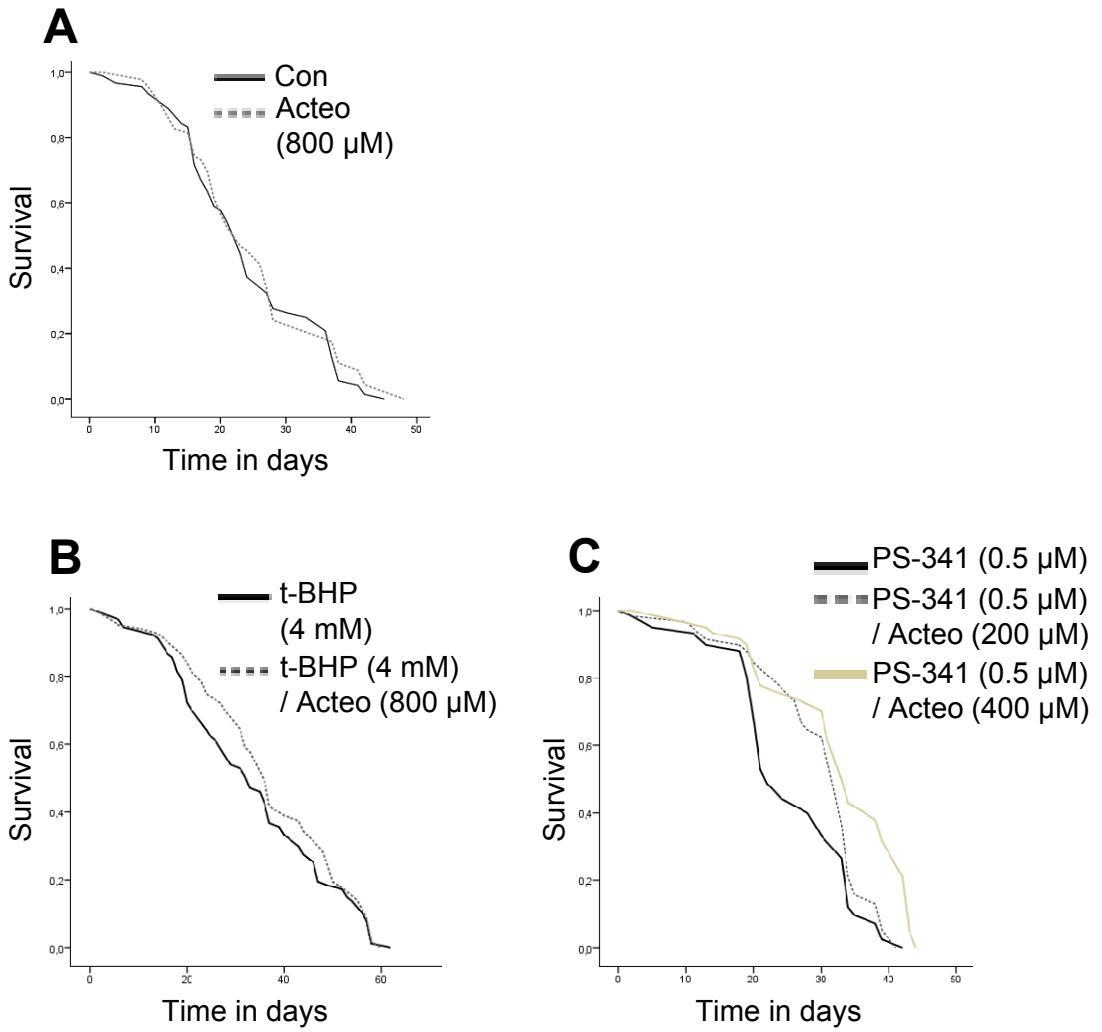

Cheimonidi et al. Fig. S9

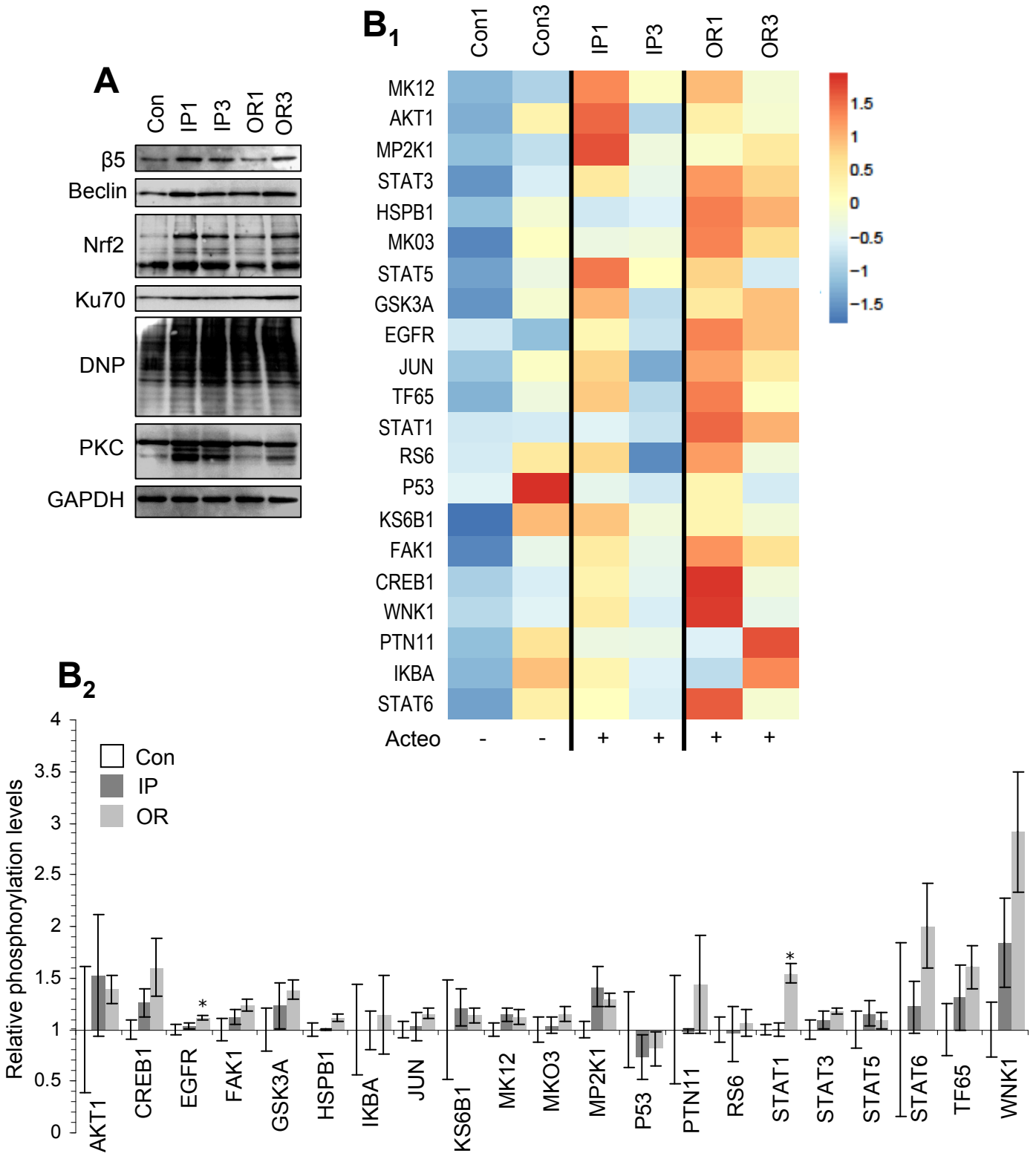

Cheimonidi et al. Fig. S10

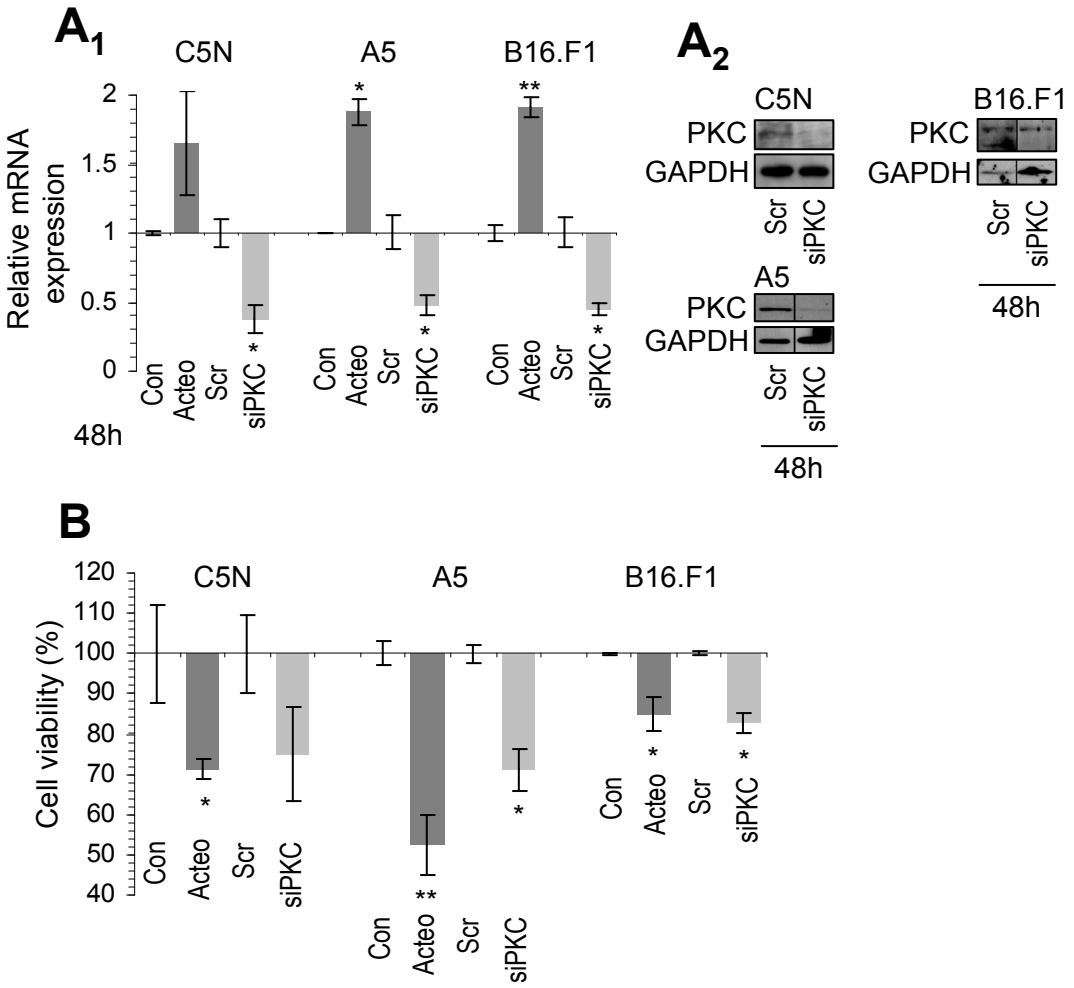

Cheimonidi et al. Fig. S11

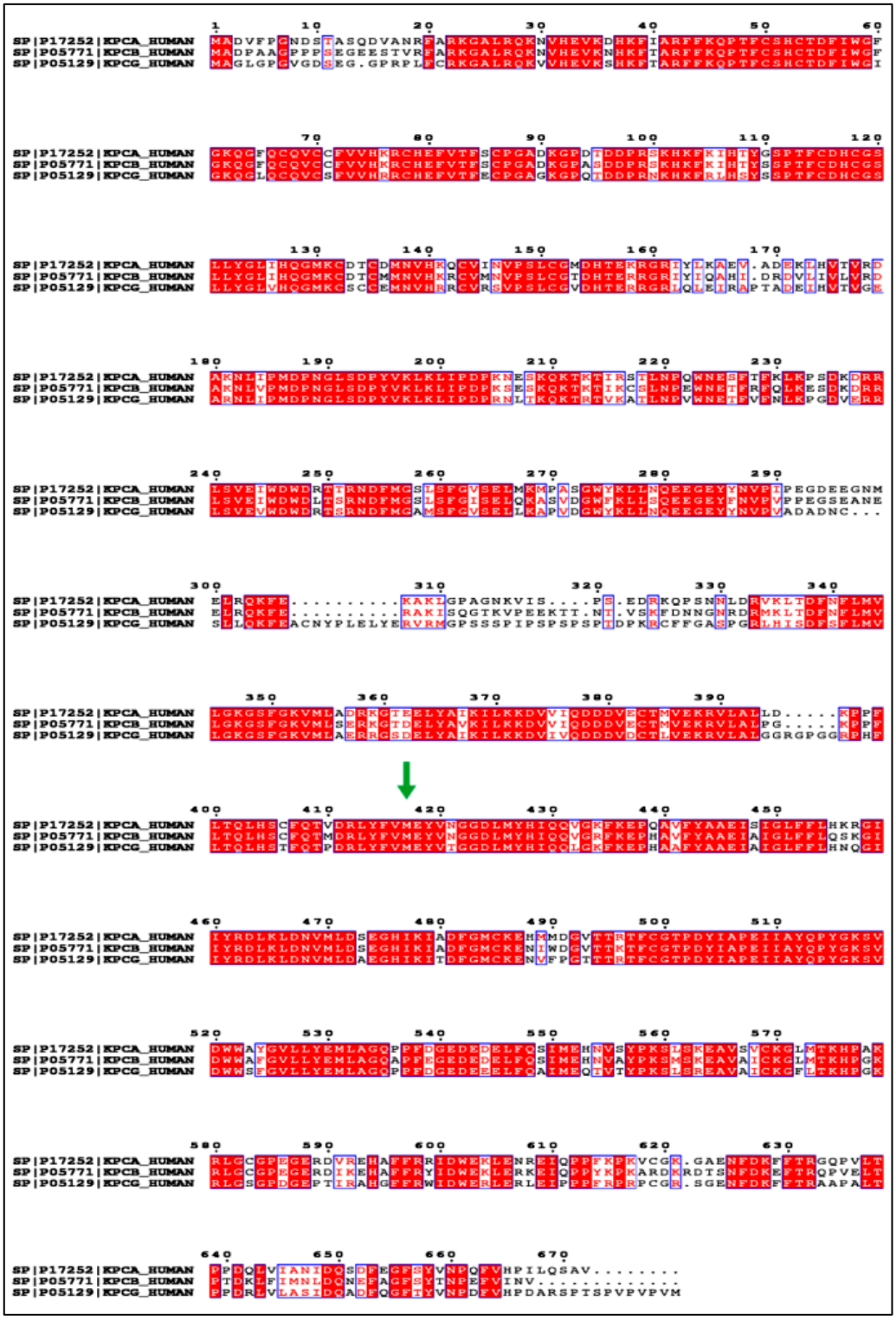

Cheimonidi et al. Fig. S12

Supplementary Table S1. Proteins analyzed for their phosphorylation status in the phosphorpoteomics platform and site of phosphorylation.

Protein	Gene name	Site of Phosphorylation
AKT1	AKT1	S473
CREB1	CREB1	S133
EGFR	EGFR	Y1068
FAK1	FAK	Y397
GSK3A	GSK3A	S21
HSPB1	HSP27	S78/S82
IKBA	IKBA	S32/S36
JUN	cJUN	S63
KS6B1	P70S6K	T389
MK12	p38g	T180/Y182
MK03	ERK1	T202/Y204
MP2K1	MEK1	S217/S221
P53	P53	S46
PTN11	SHP2	Y542
RS6	RS6	S235/S236
STAT1	STAT1	Y701
STAT3	STAT3	Y705
STAT5	STAT5	Y694
STAT6	STAT6	Y641
TF65	NFKB	S536
WNK1	WNK1	T60

Supplementary Table S2. Summary of flies' lifespan experiments.

Figure	Sample	Mean Lifespan (LF) +/- s.e.m. (Days)		Median Lifespan +/- s.e.m. (Days)		% Median LF vs. control	Max (Days)	Log Rank P Value			
								Control (DMSO)	800 µM acteoside	*Total Animals Died/Total*	
S9A	Control (DMSO)	23,833	1,097	23	1,218	100.00	45		0.509	82/90	
	800 µM Acteoside	24.6	1,187	23	2,159	100.00	48	0.509		71/87	
								4 mM t-BHP	4 mM t-BHP / 800 µM Acteoside	*Total Animals Died/Total*	
S9B	4 mM t-BHP	33,403	1,639	33	3,086	100.00	62		0.292	88/91	
	4 mM t-BHP / 800 µM Acteoside	36,703	1,706	36	1,453	109.09	60	0.292		70/82	
								PS-341 0.5 µM	PS-341 0.5 µM / Acteoside 200 µM	PS-341 0.5 µM / Acteoside 400 µM	*Total Animals Died/Total*
S9C	PS-341 0.5 µM	25,175	1,256	22	1,221	70.97	42		0.032	0.000	47/60
	PS-341 0.5 µM / Acteoside 200 µM	29,641	1,127	33	0.855	106.45	41	0.032		0.007	44/60
	PS-341 0.5 µM / Acteoside 400 µM	32.83	1,305	33	1,187	106.45	43	0.000	0.007		39/60